POSS在无铅焊点中界面反应能的分子动力学模拟

曾凡林[1], 孙 毅[1], 周 玉[2], 李清坤[2]
(1. 哈尔滨工业大学 航天科学与力学系, 哈尔滨 150001;
2. 哈尔滨工业大学 材料学院, 哈尔滨 150001)

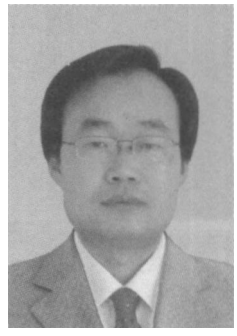

曾凡林

摘 要: 运用分子动力学模拟研究了环己烯 POSS在无铅焊点锡(β-Sn)晶体的(100)、(110)、(001)面以及在 Sn-Ag-Cu合金表面的界面反应, 得到了各自的界面反应能大小. 结果表明, 环己烯 POSS易与β-Sn的各主要晶面相结合, 但在(110)面上具有最低的界面反应能, 结合性能最好. 在锡中加入银(Ag)和铜(Cu)提高了环己烯 POSS在其表面的界面反应能, 表明对结合性能产生了不利影响, 但仍然具有较好的结合性能. 此外, 还计算了环己烯 POSS的溶解度参数. 对于理解 POSS对于无铅焊点的增强作用以及应用 POSS来开发焊料增强剂具有重要而实际的意义

关键词: 环己烯 POSS; 无铅焊点; 界面反应能; 溶解度参数
中图分类号: TG456 文献标识码: A 文章编号: 0253-360X(2010)01-0017-04

0 序 言

锡(Sn)焊是目前在电子封装领域所广泛使用的一种工程技术. 为了提高焊点的性能, 人们想出各种办法来改变焊料的成分. 一种就是所谓的混合结晶法(incorporate intermetallic). 该方法采用物理混合方法在锡金属中加入其它金属材料, 比如银(Ag)、铜(Cu)等. 这些金属能够与锡在焊接过程中发生反应产生金属间化合物(增强相)从而起到增强作用. 但是这些增强相的尺寸难以控制, 往往达到数微米, 有时反而降低了焊点的性能. 该方法对焊点性能的改善与增强相的种类、形成方法及结晶动力学密切相关, 难以控制, 因此目前在实际电子封装领域应用得并不广泛. 一种改进的方法是使增强相在焊点内尽量分散. 例如在磁场环境下往熔融的锡金属中加入其它金属离子[1]或是往熔融的锡中加入 Al_2O_3 陶瓷微粒. 但存在的问题是, 在焊点冷却过程中增强相容易生长成混杂着气孔的粗晶粒, 使增强相与锡晶体之间易于发生界面断裂从而影响焊点强度.

随着电子设备向着小型化和高集成度的发展, 纳米尺度的增强相对焊点显得尤为必要. 当增强相位于晶界时能够阻止晶界间的滑移, 从而显著提高焊点的抗热疲劳性能和工作稳定性. 类似的尝试已经应用于镍(Ni)和钴(Co)上[2]. 除了金属以外, 还有一种独特的化合物能够在焊点中形成纳米级的增强相, 这就是 POSS. POSS是多面低聚倍半硅氧烷(polyhedral oligomeric silsesquioxane)的英文简称, 它是一种具有纳米尺度的有机无机化合物, 具有无机的硅氧(Si-O)笼型结构和有机官能团[3], 这使得它既具有良好的力学性能又具有很好的化学活性, 因此被广泛应用于各种材料的化学增强相[4,5]. 同样, 当 POSS单体上含有羟基(-OH)时, 它具有与金属发生化学反应的化学活性, 可以在焊接过程中与焊点金属发生化学反应成为晶界与晶界间的“胶联剂”, 从而在焊点中形成广泛分布的增强相, 同时由于它具有天然的纳米尺寸(1.5 nm左右), 因此它还是一种优良的纳米尺度的增强相.

文献[6]将环己烯基 POSS加入到无铅焊料中使焊点的抗热疲劳性和强度有了非常显著的提高, 并且对焊点的导电性能和与基底间的结合性能没有损害. POSS在焊点中的增强效果, 涉及两方面因素: (1) POSS与金属界面间的结合能力; (2) POSS与金属原子间的化学键结合强度. 文中应用分子动力学模拟来分析 POSS在焊点中与金属界面间的界面反应能. 界面间的化学反应能的大小是衡量两界面相互结合能力的重要标准, 因此对于理解与衡量 POSS对焊点的增强效果具有重要意义.

收稿日期: 2008-09-15
基金项目: 黑龙江省科技厅国际合作资助项目(WC03112); 高校博士点基金项目(20070213054); 黑龙江省杰出青年基金; 黑龙江省自然科学基金项目(A2007-10); 哈尔滨工业大学优秀青年教师基金项目(HITQNJS.2007.002)和黑龙江省博士后基金项目(LBH-Z07151)

1 模型及模拟方法

1.1 模型

依据文献[6]选择环己烯基 POSS(cyclohexenyl-POSS)作为无铅锡焊料的增强剂,其结构式如图1所示. 焊料选择两种,一种是纯白锡焊料(β-Sn晶体),一种是 Sn-Ag-Cu合金焊料. 环己烯 POSS模型分别与 β-Sn晶体的三个典型晶面(100)、(110)、(001)和 Sn-Ag-Cu的合晶界面相接触然后进行分子动力学模拟. 图 2a是 POSS与锡晶体的(110)面相结合的分子动力学模拟初始模型. 该模型是一个含有两层物质的层状模型,下面是 Sn晶体,其下部数层原子被固定,代表晶粒具有较大的尺寸,其内部不受表面原子的影响;上面是环己烯 POSS分子附着在锡表面. 每个模型含有 8个环己烯 POSS分子. 对于不同晶面的锡晶体模型和 Sn-Ag-Cu模型来说,其原子数目有所不同. 不同模型的具体尺寸有所不同,其接触的界面面积依次为 2.332 nm×2.546 nm(100),2.546 nm×3.299 nm(110),2.332 nm×2.332 nm(001),4.97 nm²(Sn-Ag-Cu,2.181 nm×2.278 nm,非正交,夹角为 82.8°). 整个模型采用周期性边界条件并且在竖直方向具有较大的尺寸是为了使 POSS难以与晶体的下表面接近,从而只在规定的晶面上与金属发生反应.

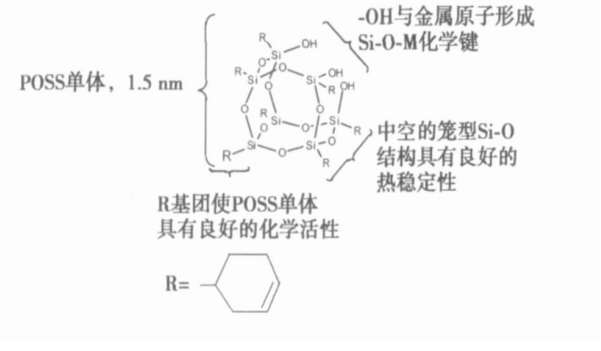

图 1 用于焊料中的 POSS结构图

Fig. 1 Structure of POSS in modification of solders

1.2 模拟方法及过程

采用 Accelrys公司的 Materials Studio软件包来进行模拟. 主要运用该软件包里的 Discover和 Amorphous Cell模块. 采用 PCFF(polymer consistent force field)分子力场[7]来计算系统的势能和原子间的作用力. PCFF通过从头计算方法得到力场参数,因此具有很高的精度和准确性. 能量和结构的优化采用 Smart Minimize方法,这是一种在优化的初始阶段采用最速下降法,在优化后期采用共轭梯度法或是 L-BFGS法[8]的智能优化方法,具有很高的精度和适应度. 温度采用 Nose-Hoover[9,10]方法来控制,因为只在 NVT系综下进行模拟,因此不涉及压力控制. 运动方程的求解采用速度— Verlet积分算法.

对上节所述的四个模型分别采用周期性边界条件在 NVT系综下以 309 K(36 ℃)的目标温度应用上述方法进行 100000步的分子动力学模拟. 积分步长取 10^{-15} s,意味着每个模型的动力学平衡时间是 10^{-10} s. 每模拟 5000步后将模型的信息进行存贮,以备提取必要的物理信息. 范德华势以原子为单位进行计算,库仑势采用 Ewald方法来计算,截断半径取 0.95 nm. 图 2b是环己烯 POSS在锡的(110)面上采用上述方法动力学模拟 100000步后的模型,可以明显看出锡的(110)表面原子发生重排, POSS的空间构型和位置也发生剧烈变化, POSS单体与锡表面发生作用,两者相互靠近,并且出现部分原子的相互渗入.

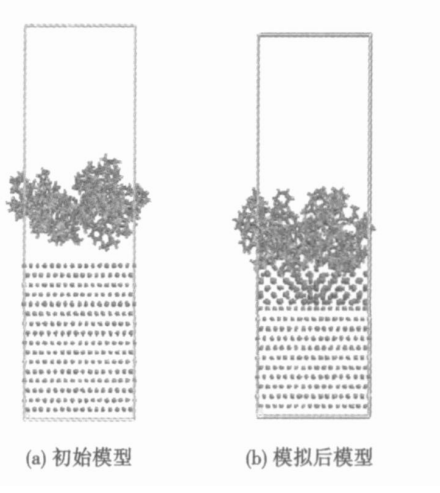

图 2 POSS与锡界面反应的模拟模型

Fig. 2 Simulation model of interface interaction between POSS and Sn crystal

2 计算结果

2.1 环己烯 POSS的溶解度参数

为了验证 PCFF力场的可靠性,首先计算了水和环己烯 POSS的溶解度参数. 对于 POSS来说,粘着性(内聚性)是很重要的性能参数但很难通过试验来测量. 而溶解度参数由内聚能密度(J_{ED})来计算[11]. 在分子动力学模拟中,内聚能 E_{coh}是使分子聚集在一起的作用能,定义为当将所有分子间作用能除去时每摩尔物质所增加的势能. 对应地, J_{ED}是

指单位体积内的内聚能大小. 如果设 V_{mol}为一摩尔某物质的体积, I_{CED}可定义为

$$I_{CED} = (E_{coh} / V_{mol}) \quad (1)$$

溶解度参数 δ定义为 I_{CED}的平方根，故

$$\delta = (E_{coh} / V_{mol})^{1/2} \quad (2)$$

通过计算得到水在 300 K下的 I_{CED}为 5.12×10^8 cal/m³，其溶解度参数为 22.6 (cal/cm³)$^{1/2}$，与试验值 23.4相当接近. 同样方法得到环己烯 POSS在 309 K下的 I_{CED}为 5.20×10^7 cal/m³，其溶解度参数为 7.21. 这表明环己烯 POSS非常难溶于水，而易溶于正己烷 (溶解度参数 7.3)和乙醚 (溶解度参数 7.4). 同样地，对溶解度参数的模拟也证明 PCFF力场的可靠性，为界面反应能的计算提供了可靠的依据.

2.2 环己烯 POSS与 Sn的 (100)面及 (110)面和 (001)面的界面反应能

界面反应能密度 $E_{adhesion}$通过下列公式来计算，即

$$E_{adhesion} = \frac{E_{total} - (E_{surface} + E_{POSS})}{S} \quad (3)$$

式中：E_{total}是环己烯 POSS和锡组成的系统的总能量；$E_{surface}$是将环己烯 POSS移除后剩下的锡晶面的能量；E_{POSS}是将锡晶面移除后剩下的环己烯 POSS的能量；S表示两者接触的界面面积. 文献 [12]用有机材料的体积 V代替上式中的 S来计算单位体积内的界面反应能. 但是在文中，尽管各模型所含有的环己烯 POSS的数目和体积相同，但因为不同的锡的界面模型具有不同的界面面积，因此环己烯 POSS与各晶面的接触面积有所不同，因此界面反应能也有所不同. 为了使不同模型之间的计算结果具有对比性，计算单位面积上的界面反应能. 锡的 (100)面模型如图 3所示.

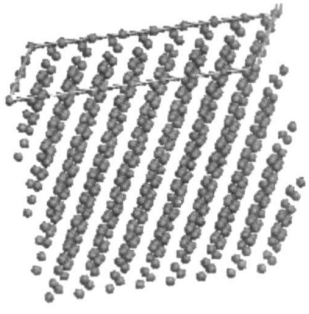

图 3　锡的 (100)面模型

Fig. 3　Model of (100) plane of Sn

将图 3与环己烯 POSS所组成的层状模型首先进行能量最小化的优化之后，按 1.2节所述的方法进行分子动力学模拟. 其界面反应能 $E_{adhesion}$与模拟时间的关系如图 4所示. 可以看出在整个动力学模拟过程中，$E_{adhesion}$都为负值，表明环己烯 POSS能够与锡的 (100)面很好地结合.

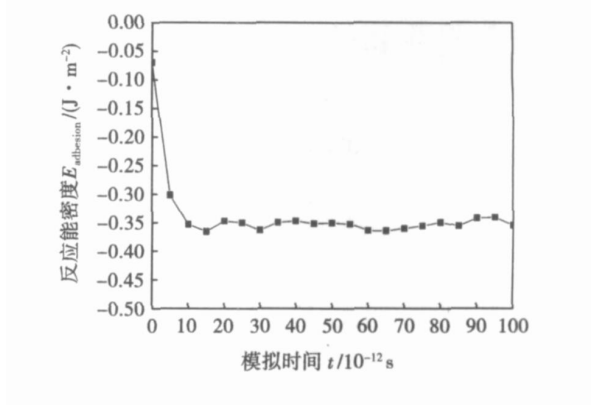

图 4　环己烯 POSS在锡的 (100)面上的界面反应能变化

Fig. 4　$E_{adhesion}$ evaluation of cyclohexenyl-POSS on (100) plane of Sn

同理，环己烯 POSS在锡的 (110)面和 (001)面上的界面反应能与模拟时间的关系分别如图 5和图 6所示. 从两图可以明显看出，$E_{adhesion}$也都小于零，表明环己烯 POSS在锡的 (110)面和 (001)面上也都能与之很好地结合.

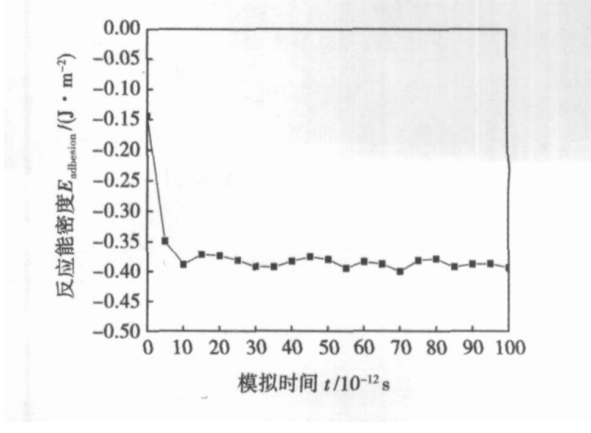

图 5　环己烯 POSS在锡的 (110)面上的界面反应能变化

Fig. 5　$E_{adhesion}$ evaluation of cyclohexenyl-POSS on (110) plane of Sn

2.3 环己烯 POSS与 Sn-Ag-Cu合金的界面反应能

在 Andre等人[6]的试验中，环己烯 POSS除了加入到纯锡焊料中以外，还加入到 Sn-Ag-Cu合金焊料中，也使得焊点的性能得到了大幅度提高. 为了计算环己烯 POSS与 Sn-Ag-Cu合金的界面反应能，采用 Ag 3.8%，Cu 0.7%，Sn 95.5%这一实际工程比例[13] (欧盟推荐)来构建合金模型. 为了近似地

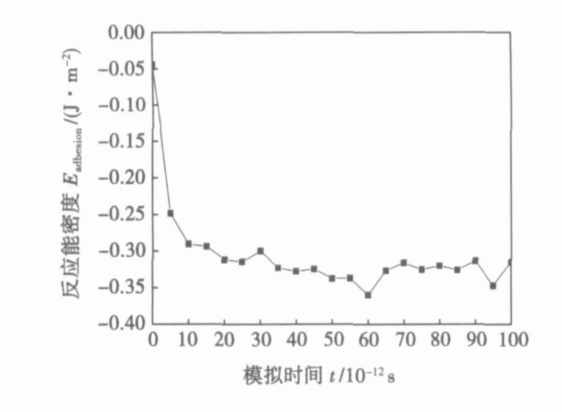

图 6 环己烯 POSS在锡的(001)面上的界面反应能变化

Fig. 6 $E_{adhesion}$ evaluation of cyclohexenyl-POSS on (001) plane of Sn

达到这一比例,选择含有 128个 β-Sn晶胞的晶格模型,24个 Ag原子和 8个 Cu原子分别原位替代模型中的 Sn原子. 按照 Chun等人[14]的方法, Ag原子取代中心 Sn原子的位置,而 Cu原子则取代既非中心亦非边界处的 Sn原子的位置. 将模型进行能量最小化并优化模型结构后得到界面尺寸为 2.181 nm ×2.278 nm,并且晶体结构不再正交. 最终得到的模型如图 7所示.

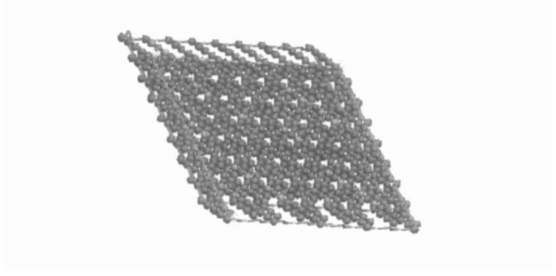

图 7 Sn-Ag-Cu合金模型

Fig. 7 Model of Sn-Ag-Cu alloy

将图 7所示模型与 8个环己烯 POSS所组成的层状模型首先进行能量最小化的优化之后,按 1.2节所述的方法进行分子动力学模拟,然后计算界面反应能密度 $E_{adhesion}$. 图 8为环己烯 POSS在 Sn-Ag-Cu表面的界面反应能密度 $E_{adhesion}$与模拟时间的关系. 从图 8中可以看到,虽然 $E_{adhesion}$比在锡的(100)面、(110)面和(001)面都要高,但都小于零,表明在 Sn-Ag-Cu合金中,环己烯 POSS也能很好地与晶面相结合.

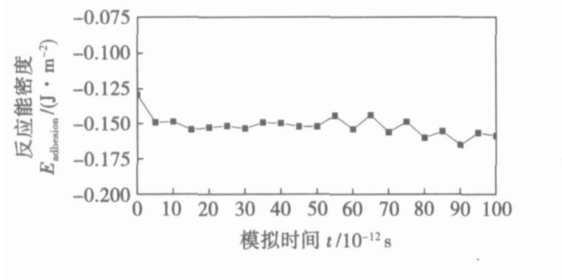

图 8 环己烯 POSS在 Sn-Ag-Cu表面的界面反应能变化

Fig. 8 $E_{adhesion}$ evaluation of cyclohexenyl-POSS on surface of Sn-Ag-Cu alloy

3 讨 论

为了使结果更加合理,分别只取上述结果的后面 50 000步,消除模拟的前半部分由于平衡不充分所带来的影响,即每组结果只取后面的 10个有效数值的平均值,所得到的结果列于表 1中.

表 1 环己烯 POSS在各个界面上的界面反应能密度

Table 1 $E_{adhesion}$ of cyclohexenyl-POSS on different surfaces

晶体界面	反应能密度 $E_{adhesion}$/(J·m^{-2})
Sn(100)	−0.354 05 (0.008 216)
Sn(110)	−0.387 84 (0.006 685)
Sn(001)	−0.330 92 (0.014 533)
Sn-Ag-Cu	−0.153 7 (0.006 758)

注:括号内数值表示标准差

从表中数值可以看出,环己烯 POSS在锡的(110)面上的界面反应能密度最低,意味着在实际焊点中,环己烯 POSS最容易结合在锡的(110)面上. 然后依次是(100)面和(001)面. 不过总的来看,在锡的三个主要晶面上,环己烯 POSS都具有较低的界面反应能,且相互差别不大,表明环己烯 POSS能够较均匀地分布于锡多晶的晶面上,并且容易与之结合. 而对于 Sn-Ag-Cu合金来说,从计算结果来看,加入了银和铜以后,显然对环己烯 POSS在晶面上的界面反应能产生了明显的影响. 环己烯 POSS在 Sn-Ag-Cu合金表面的界面反应能相对于锡多晶来说至少提高了 50%,显然银和铜的加入,降低了环己烯 POSS在锡晶面上的结合性能. 不过其界面反应能密度仍然为 −0.1537 J/m^{2}的低值,表明环己烯 POSS仍然能够很好地与界面相结合.

此外,在 2.1节得到的环己烯 POSS的溶解度参数表明其极难溶于水,但易溶于正己烷和乙醚等溶剂. 而正己烷正是无铅电子工艺中常用的有机溶剂. 这表明在焊接过程中,环己烯 POSS易溶于有机溶剂从而能够顺利填充到晶体的界面中去,这一特性为利用环己烯 POSS来增强焊点的强度制造了有利条件.

4 结 论

(1)环己烯 POSS与锡的各主要晶面都具有较

[下转第 24页]

表 3 不同焊接速度下近似熵均值及标准差和熔滴过渡频率

Table 3 Mean $<A_E>$ and its standard deviation $\sigma(A_E)$ and droplet transfer frequency f at different welding speeds v_w

焊接速度 v_w/(cm·min^{-1})	近似熵均值 $<A_E>$	近似熵标准差 $\sigma(A_E)$	熔滴过渡频率 f/Hz
21	0.457 8	0.031 0	103
24	0.452 8	0.033 5	105
27	0.475 0	0.027 9	103
30	0.528 5	0.023 0	111
33	0.499 4	0.020 8	110
36	0.474 2	0.060 4	112
39	0.465 9	0.054 6	110
42	0.461 3	0.068 9	109

4 结 论

(1)物理试验和数值分析证明在改变 U_a 的条件下, A_E 越大, 越高, 焊接过程越稳定.

(2)在分别改变 和 v_w 的情况下, A_E 仍与焊接过程稳定性成正相关关系, 但 却变化甚微, 难以反映焊接过程稳定性的动态变化, 因此 A_E 比 更全面准确刻画了 CO_2 短路过渡过程稳定性的动态变化, 用于定量表征焊接系统的稳定性时优于 .f

参考文献:

[1] Pincus S M. Approximate entropy as a measure of system complexity[C]// Proceedings of the National Academy Sciences of the United States of America. Melville NY 1991: 2297—2301.

[2] Pincus S M. Approximate entropy (AE) as a complexity measure [J]. Chaos, 1995, 5(1): 110—117.

[3] 殷树言. 气体保护焊工艺基础[M]. 1版. 北京: 机械工业出版社, 2007.

作者简介: 向远鹏, 男, 1971年出生, 博士, 讲师. 主要从事电力电子装置与电能变换技术的科研和教学工作. 发表论文 8篇.

Email: xiangyp519@qq.com

[上接第 20页]

低的界面反应能, 表明环己烯 POSS与锡的各主要晶面都有良好的结合性能, 但在其(110)面上结合性能最好.

(2) Sn-Ag-Cu合金焊点中, 环己烯 POSS与合金表面的界面反应能高于纯锡表面的界面反应能, 表明银和铜影响了环己烯 POSS与锡的结合性能, 但结合性能依然较好.

(3)结果对于理解 POSS对焊点的增强作用以及应用 POSS来开发焊料增强剂具有实际意义.

参考文献:

[1] Mavoori H, Jin S. New creep-resistant low melting point solders with ultrafine oxide dispersions[J]. Journal of Electronic Materials, 1998, 27(11): 1216—1222.

[2] Chen C M, Chen S W. Electromigration effect upon the Sn-0.7 wt% Cu/Ni and Sn-3.5 wt% Ag/Ni interfacial reactions[J]. Journal of Applied Physics, 2001, 90(3): 1208—1214.

[3] Sckwab J J, Lichtenhan J D. Polyhedral oligomeric silsesquioxane (POSS)-based polymers[J]. Applied Organometallic Chemistry, 1998, 12(10—11): 707—713.

[4] Li G Z, Wang L, Toghiani H, et al. Viscoelastic and mechanical properties of vinyl ester (VE)/multifunctional polyhedral oligomeric silsesquioxane (POSS) nanocomposites and multifunctional POSS-styrene copolymers[J]. Polymer, 2002, 43(15): 4167—4176.

[5] Xu H Y, Kuo S W, Chang F C. Significant glass transition temperature increase based on polyhedral oligomeric silsequioxane (POSS) copolymer through hydrogen bonding[J]. Polymer Bulletin, 2002, 48(6): 469—474.

[6] Andre L, Subramanian K N. Development of nano-composite lead-free electronic solders[J]. Journal of Electronic Materials, 2005, 34(11): 1399—1407.

[7] Sun H. Ab initio calculations and force field development for computer simulation of polysilanes[J]. Macromolecules, 1995, 28(3): 701—712.

[8] Nocedal J. Updating quasi-newton matrices with limited storage [J]. Mathematics of Computation, 1980, 35: 773—782.

[9] Hoover W G. Constant pressure equation of motion[J]. Physics Review A, 1986, 34(3): 2499—2503.

[10] Nose S. A molecular dynamics method for simulations in the canonical ensemble[J]. Molecular Physics, 1984, 52(2): 255—268.

[11] Bicerano J. Prediction of polymer properties[M]. New York: Marcel Dekker Inc, 1993.

[12] Prathab B, Subramanian V, Aminabhavi T M. Molecular dynamics simulations to investigate polymer-polymer and polymer-metal oxide interactions[J]. Polymer, 2007, 4: 409—416.

[13] Kim K S, Huh S H, Suganuma K. Effects of intermetallic compounds on properties of Sn-Ag-Cu lead-free soldered joints[J]. Journal of Alloys and Compounds, 2003, 352(1—2): 226—236.

[14] Chun Y, Hao L. First principles calculations of the effects of Cu and Ag additions on the electromigration of Sn-based solder[J]. Journal of Applied Physics, 2007, 102(5): 1—4.

作者简介: 曾凡林, 男, 1978年出生, 工学博士, 讲师. 主要从事纳米复合材料力学、微纳米力学方面的科研和教学工作. 发表论文 20余篇.

Email: zengfanlin@hit.edu.cn

MAIN TOPICS, ABSTRACTS & KEYWORDS

Distributive characteristic of stress field in electron beam welded joint of TiAl intermetalics plates CHEN Guoqing, ZHANG Binggang, LIU Wei, FENG Jicai, LIU Yulong (National Key Laboratory of Advanced Welding Production Technology, Harbin Institute of Technology, Harbin 150001, China). p 1—4

Abstract: Welding stress in electron beam welding joint of TiAl intermetalics plates, as well as the relationship between stress distribution and crack characteristic were numerical stimulated using thermo-elastic-plastic finite element method. The results showed that stress σ_x along welding direction was tensile stress, and which was a relatively high level in central weld. With the highest value of 390 MPa. σ_x in the cross section in central weld was tensile stress and it came to the largest value of 415 MPa in HAZ. In the same section, σ_y perpendicular to welding direction was also tensile stress and the largest value was approximately to 160 MPa at the site 1.9 mm away from weld center line. The highest tensile strength of the joints welded under different heat inputs was 304.7 MPa. Fracture occured near HAZ, e.g. the place where the residul stress value was the largest from the numerical simulation results.

Key words: TiAl intermetalics plates; electron beam welding; stress field distribution

Microstructure and hardness of laser welded joint of China low activation martensitic steel LEI Yucheng, HAN Mingjuan, ZHU Qiang, JU Xin[2] (1. School of Material Science and Engineering of Jiangsu University, Zhenjiang 212013, Jiangsu, China; 2. Physics Department, University of Science and Technology of Beijing, Beijing 100083, China). p 5—8

Abstract: Laser welding of 6mm-thick CLAM is conducted with different welding parameters by 4 kW Nd:YAG. Microstructure and hardness of welded joint are analyzed with pre- and post tempering respectively. The results show that the microstructure of welded joints are mainly coarse lath martensite and hardness of welded joint is increased as welding speed rises before tempering. After tempering, microstructure of welded joint is tempered lath martensite. A large amount of carbide particles are observed in original austenite grain boundary and martensite lath by SEM, which lead to a slight increase in the hardness of weld zone to base metal relatively. HAZ is not softened.

Key words: low activation martensitic steel; CLAM; YAG laser welding; microstructure; hardness

Analysis on mechanism of laser-assisted TIG arc ignition XIA Yuan, SONG Yonglun, RAN Guowei, SHI Linan (Department of Mechanical Engineering & Applied Electronics Technology, Beijing University of Technology, Beijing 100124, China). p 9—11, 16

Abstract: Laser-assisted TIG arc ignition was applied by 1000W semiconductor laser. Using emission spectroscopy method, the arc ignition process of the spectral information at different moments was observed, while the transient characteristics of electron density were obtained by Stark broadening method. The results show that in the arc ignition process, the contribution of electron from different elements is obviously different. In the beginning of arc ignition, the contribution of electron was from the ionizing metallic element, as time increasing, the contribution of electron from gas was gradually increased, and for the existence of the electric field between electrodes, high-temperature gas quickly formed a cascade of ionizing and finally arc was established.

Key words: laser; TIG arc; arc ignition; spectral diagnosis; mechanism

H_2S stress corrosion invertigation of pipeline steel welded joints XU Lianyong[1,2], JING Hongyang[1,2], CAO Jun[3], LI Chunguo[3], SUN Youhui[3] (1. School of Materials Science and Engineering, Tianjin University, Tianjin 300072, China; 2. Tianjin Key Laboratory of Advanced Joining Technology, Tianjin 300072, China; 3. Offshore Oil Engineering Co. Ltd, Tianjin 300452, China). p 12—16

Abstract: The H_2S stress corrosion tests were conducted for the welded joints of X56 steel and X65 steel under various welding processes in order to investigate the susceptibility of weld metal and heat-affected zone (HAZ) to H_2S stress corrosion cracking (SCC), and the wedge-opening loading (WOL) specimens were used in the tests. The test results showed that small crack growth occurred in all specimens, and the crack stopped to grow when the stress intensity factor K reached the critical value (threshold stress intensity factor). In this paper, the H_2S stress corrosion resistance of HAZ was better than that of weld metal for the welded joints of X56 and X65 steel. In addition, the corrosion resistance of HAZ and weld metal were worse than that of base metal inferred to literature, which was caused by grain growth coarsening, welding residual stress of HAZ and weld metal, weld strength overmatching and welding defects.

Key words: stress corrosion; welded joint; pipeline steel; critical stress intensity factor

Molecular dynamics simulations of interface interactions of POSS in lead free solder joints ZENG Fanlin[1], SUN Yi[1], ZHOU Yu[1], LI Qingkun[2] (1. Department of Astronautic Science and Mechanics, Harbin Institute of Technology, Harbin 150001, China; 2. Material Science and Engineering, Harbin Institute of Technology, Harbin 150001, China). p 17—20

Abstract: The interface interactions of cyclohexenyl-

POSS on the (100), (110) and (001) planes of the lead free solder joints β-Sn and on the surface of the Sn-Ag-Cu alloy were performed via the molecular dynamics (MD) simulations. The cohesive energies were also obtained. The results show that the cyclohexenyl-POSS can be easily absorbed on the main crystal planes of β-Sn. But the cohesive energy on (110) plane is the lowest, thus the cyclohexenyl-POSS will be absorbed on the (110) plane most likely. Adding the silver (Ag) and the copper (Cu) into β-Sn to form the Sn-Ag-Cu alloy raises the cohesive energies of cyclohexenyl-POSS on the alloy surfaces and generate the unfavorable absorbing effect. But the cyclohexenyl-POSS can also be easily absorbed on the surfaces. Moreover, the solubility parameter of the cyclohexenyl-POSS was computed from the MD simulations.

Key words: cyclohexenyl-POSS; lead free solder joints; cohesive energy; solubility parameter

Effects of approximate entropy and droplet transfer frequency on process stability of CO_2 short-circuiting welding

XIANG Yuanpeng, CAO Biao (1. School of Mechatronics Engineering, University of Electronics and Science Technology of China, Chengdu 611731, China; 2. School of Mechanical and Automotive Engineering, South China University of Technology, Guangzhou 510641, China). p21—24

Abstract: Based on the experimental time series of welding current produced by CO_2 welding with short-circuiting transfer under different arc voltages, gas flow rates and welding speeds, the approximate entropy of the welding current has been numerically evaluated by the implementation of Pincus's algorithm. The different effects of approximate entropy and droplet short-circuiting transfer frequency on the welding process stability are also analyzed. Experiments and numerical analysis demonstrate that approximate entropy reaches larger values when the welding processes approach more steady states under the condition of the three above-mentioned process experiments. The variation trend of the droplet short-circuiting transfer frequency is not always consistent with that of welding process stability. So approximate entropy characterizes the welding process stability more accurate than the droplet transfer frequency.

Key words: CO_2 short-circuiting weld; approximate entropy; droplet trarsfer frequency

RSW fuzzy artificial neural network control method based on variable universe

YUAN Qingke, SHI Yaping, ZHANG Mingtian, FENG Sang (College of Mechanical & Electrical Engineering, Guangdong University of Technology, Guangzhou 510006, China). p25—28, 32

Abstract: In order to enhance the control precision and welding quality of resistance spot welding (RSW), according to the RSW control characteristics, it put forward the RSW fuzzy artificial neural network (FANN) control method based on variable universe by integrating the variable universe technology and FANN. The network structure of FANN was designed and the process of neural computation dealing with the fuzzy, the fuzzy rules and the solution of fuzzy was analyzed. And the method of how to fix on the extension-contraction factors of input and output universe was researched. Then a kind of FANN controller of RSW with the variable universe was developped, being applied to a kind of spot welding experiments to study and analyze. The results prove the FANN control method is better than other fuzzy control methods.

Key words: fuzzy control; spot welding; artificial neural network; variable universe; extension-contraction factors

Influence of electrochemical reaction on oxygen pick-up for droplet metal in direct current welding

LI Xiaoquan, CHU Yajie, YANG Zonghui (School of Material Engineering, Nanjing Institute of Technology, Nanjing 211167, China). p29—32

Abstract: On the basis of oxygen pick-up dynamic analysis in droplet metal, a series of self-made agglomerative fluxes with different basicity indexes were used by the droplet metal on water cooled copper with no weld pool adopting direct current submerged arc welding, so as to obtain some quality and geometric messages contained in droplet metal for its oxygen pick-up analysis resulted from electrochemical reaction. The results show that with the increase of slag basicity index, eletrochemical reaction occurring at the interface of slag-metal would be more obvious, and so is the amount of oxygen gaining from electrochemical reactuon. For $CaO-Al_2O_3-SiO_2$ slag in this study, the extend of oxygen gaining from electrochemical reaction can be almost equal to that from thermo-chemical, therefore it is an in-negligible oxygen induced factor in formulating direct current welding technology or developping high basic index welding consumables.

Key words: electrochemical reaction; direct current welding; droplet metal; induced oxygen; basicity index

M_7C_3-type carbide and abrasion resistance of Fe-C-Cr-V high chromium hardfacing alloys

GONG Jianxun, XIAO Yifeng, ZHANG Qinghui, MA Mo (1. School of Mechanical Engineering, Xiangtan University, Xiangtan 411105, Hunan, China; 2. Faculty of Material and Photoelectronic Physics, Xiangtan University, Xiangtan 411105, Hunan, China). p33—36

Abstract: High chromium hardfacing alloys containing 0.9-3.0% C, 15-20% Cr, 2.0-3.0% V (wt%) were deposited by flux-cored wire submerged arc welding (SAW). The microstructure and carbide morphology were investigated by optical microscopy (OP), scanning electron microscopy (SEM) and X-ray diffraction (XRD). The microstructure consists of martensite, ferrite and austenite carbide such as primary M_7C_3, $(Fe,Cr)_3C$ and TiC etc. Orientational M_7C_3-type carbide grains distributing in the plane vertical to the hardfacing surface were obtained by the optimization of flux-cored wire and welding speed. The analysis of energy dispersive spectrometer (EDS) indicated that M_7C_3 type carbide was $(Fe,Cr,V)_7C_3$. In addition, the effects of carbon content on hardness and wear properties were evaluated. Experimental results demonstrated that the abrasion re-